KSME Journal, Vol. 1, No. 2, pp. 147~157, 1987.

A LAGRANGIAN MODEL FOR SPRAY DRYER DESULFURIZATION SYSTEM

Sung Joon Kim*

(Received August 31, 1987)

The purpose of this work is to develop a reliable numerical model for the spray dryer desulfurization system. The shape of the spray dryer requires that a body fitted orthogonal coordinate system be used for the numerical model. The governing equations are developed in the general orthogonal coordinates and discretized to yield a system of algbraic equations. A modified two-equation turbulence model is also included in the numerical program. The stability of QUICK scheme is investigated and the Absolutely Stable QUICK scheme is developed and included in the numerical model. The trajectory approach is used to simulate the flow of the dispersed phase. Two-way coupling phenomena is modeled by this sheme. The absorption of sulfur dioxide into lime slurry droplets is simulated by a model based on gas-phase mass transfer. The program is applied to a typical spray dryer desulfurization system. The reuslts show the capability of the program to predict the sensitivity of system performance to change in operational parameters.

Key Words: Lagrangian Model, Numerical Scheme, Desulfurization System, PSI-CELL Scheme.

1. INTRODUCTION

The increasing cost of energy encourages the use of coal in place of petroleum as an energy source. Coal, though inexpensive, has the disadvantage of producing pollutants during the burning process. As coal consumption is increased, the need for means to remove pollutants such as sulfur dioxide from flue gas is intensified.

There are basically two ways of removing sulfur dioxide from flue gases: dry scrubbing and wet scrubbing. Desulfurization by dry scrubbing has several advantages over wet scrubbing even though it has generally lower efficiency than wet scrubbing. These advantages include simpler waste disposal, less complex operation, lower capital cost, and lower operating cost and maintenance. These advantages have enhanced the interest in spray dryer flue gas desulfurization (spray dryer F. G. D.).

A typical system for a spray dryer F. G. D. is shown in Fig. 1. It consists of slurry preparation equipment, dust collection equipment and a spray dryer. The process is initiated by mixing lime and water and pumping the slurry to an atomizer. The atomizer produces a cloud of droplets which are upon previous experience and pilot plant tests. The use of pilot plant studies to guide the design and to determine the influence of operating parameters is extremely costly. Also, the results from pilot plant studies can be difficult to interpret if the controlling physical phenomena have not been identified.

A reliable numerical model of spray dryer F. G. D. would be a valuable asset to system design. Such a model would reduce the need for expensive pilot plant studies and would complement design.

A nurmerical model for spray dryer F. G. D. (O'Rourke, 1982) has been developed by the Los Alamos Laboratory in 1982. This code (called the LDEF program) uses the SOLA algorithm as modified by Dukowicz (Dukowicz, 1980). The numerical accuracy is only first order. LDEF code does not include the SO_2 absorption process. It has several problems which must be solved before it can be regarded as more than a numerical experiment, one being the enormous reguirement in run time and storage. A run of LDEF requires more than two hours of CDC 7600 computer time (Christian, 1982). It is not useful until it includes an appropriate model for SO_2 removal from the flue gas. The turbulent model in LDEF is very simplistic in that it is based on a constant effective viscosity. The computational grid system is not a body-fitted

because of numerical diffusion along the converging wall.

Based on a review of the literature, there seems to be a need for a numerical model which adequately models the physics of the spray dryer F. G. D. process and can be conveniently used to complement design. The objective of this study is to develop a numerical model for spray dryer F. G. D. which can be used reliably and efficiently to complement industrial design.

2. NUMERICAL SIMULATION OF CONTINUOUS PHASE

There are sveral advantages in using curvilinear orthogonal coordinates for developing a numerical model of internal curvilinear computational grid lines align more closely with the stream lines of fluid flow than rectangular grid lines. The curvilinear grid lines can also be refined more easily near the walls where gradients are large. The numerical simulations of boundary conditions on the curved surfaces are also more easily expressed with a curvilinear grid system than with a rectangular system. Even though these advantages are available with a curvilinear grid system, still, the adoption of a curvilinear grid system reguires a scheme to generate computational grid lines and the use of governing equations based on a curvilinear coordinate system.

2.1 Generation of General Orthogonal Grid System

Generation of a general orthogonal grid system is done by a computational program developed by Murthy (Murthy, 1981). In Murthy's program, the grid lines are treated as equipotential lines corresponding to two potential functions, $\phi(x, y)$ and $\Psi(x, y)$, defined in the domain of the flow region which satisfy:

$$\nabla^2\phi=0 \qquad \nabla^2\Psi=0 \tag{1}$$

The computational grid points are the points of intersection of iso-ϕ and iso-Ψ lines. Solving Eq. (1) with appropriate boundary conditions yields $\phi(x, y)$ and $\Psi(x, y)$. Interpolation is required to determine the X-Y coordinates of intersection points between iso-ϕ and iso-Ψ lines. There is another way which obviates these interpolations, which is the solution of the inverse problem for $x(\phi, \Psi)$ and $y(\phi, \Psi)$. The inverse equations are obtained by using the general transformation. The inverse equations are solved with the appropriate boundary conditions. An orthogonal grid system generated by the program is shown in Fig. 2.

2.2 Development of Governing Equations

Pope (Pope, 1978) derives the governing equations in general orthogonal coordinates from equations in Cartesian coordinates by mathematical coordinate transformations. However, it is very difficult to identify the physical meaning of each term in the derived equations. Another method, shown here, is to develop the governing equations in general orthogonal coordinates from the basic physical laws using the control volume approach. It allows one to more easily indentify the physical meaning of each term in the equations. The governing equations and constitutive equations are formulated for axisymmetric, swirling, turbulent flow inside the spray dryer F. G. D. The following notations and drawings are used for the development of governing and constitutive equations. The three axes of a general orthogonal coordinate system, shown in Fig. 3, are denoted by ξ, η and ζ, respectively. The quantities $\ell_\xi d\xi$, ℓ_η and $\ell_\zeta d_\zeta$ represent the infinitesimal length in the ξ, η and ζ directions, respectively. The variables ℓ_ξ, ℓ_η and ℓ_ζ are called stretching factors. A control volume can be drawn as shown in Fig. 4 with the notations defined above. The radii of curvature are expressed by r_ξ r_η, $r_{\zeta\xi}$ and $r_{\zeta\eta}$ which are illustrated in Fig. 5. and Fig. 6. The

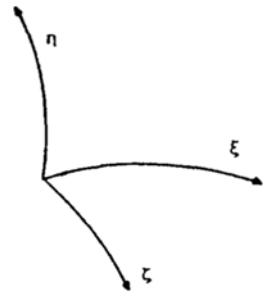

Fig. 3 General orthogonal coordinates

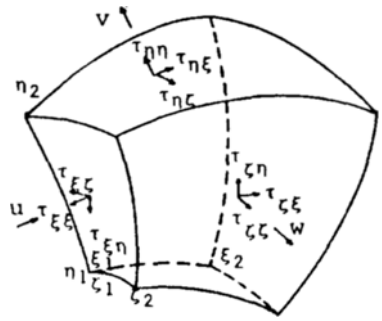

Fig. 4 Control volume and stresses

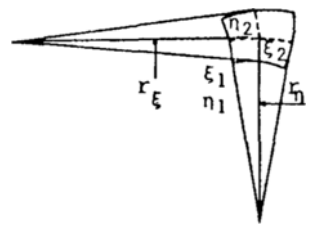

Fig. 5 Radii of curvature

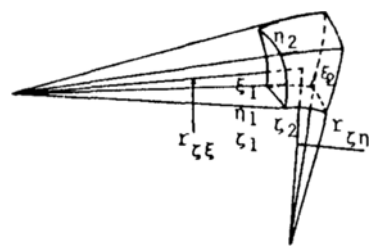

Fig. 6 Radii of curvature

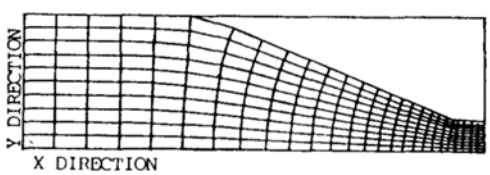

Fig. 2 Computational grid system

radii r_ξ and r_η are associated with ξ-η plane and $r_{\xi\eta}$ and $r_{\xi\xi}$ are in the ξ-ζ plane and the η-ζ plane, respectively. In axisymmetric flow, there are six shear stress $\tau_{\xi\xi}$, $\tau_{\eta\eta}$, $\tau_{\zeta\zeta}$, $\tau_{\xi\zeta}$, $\tau_{\xi\eta}$ and $\tau_{\eta\zeta}$, that act on the fluid element. The stresses τ_{rr} and $\tau_{\eta\eta}$ stretch the fluid element and $\tau_{\xi\eta}$, $\tau_{\xi\zeta}$ and $\tau_{\eta\zeta}$ affect shear strains. These stresses are illustrated on the control volume shown in Fig. 4.

A series of equations are presented in Appendix A. They include the constitutive equations, the continuity equation, the general trasport equation, the momentum equation and the thermal energy equation. The constinuity equation in steady state is derive from the law of mass conservation. The control volume shown in Fig. 4 is used to formulate this equation. There is no net mass flux in the ζ direction due to the symmetry assumption. A general scalar transport equation in steady state differs from the coantinuity equation through the diffusion terms of a scalar quantity. Momentum equations in the steady state are developed from the Newton's second law by using Reynolds transport theorem for the control volume. The energy conservation law is applied to the field in the control volume in order to obtain the thermal energy equation.

The two-equation turbulence model (K-ε model modified with streamline curvature effect (Benodekar, 1983)) is adopted to simulate the flow phenomena of the continuous phase. The generation of turbulent energy in the turbulent kinetic energy equation is formulated in general orthogonal coordinates.

2.3 Numerical Scheme (Absolutely Stable QUICK)

An absolutely stable numerical scheme is introduced and tested in this section. It is proved through mathematical theory and numerical experiments that this scheme has feasible numerical properties.

Numerical properties, here, refer to mainly computational accuracy and numerical stability. Numerical accuracy is usually defined by trunction errors in Taylor series approximations of the dependent variable. More accurate numerical solutions can be obtained by using higher order approximations of dependent variables. But increasing accuracy in numerical schemes raises several disadvantages such as increased computational cost, instability and difficulties in simulating boundary conditions.

Stability is a crucial property in numerical schemes. One can not obtain a solution with good stability properties of a numerical scheme because deviations generated during iteration are not damped out but augmented. For stability analyses, the analogy between the iterative solution of the elliptic equations and the time-dependent solution of parabolic equations can be used (Neuberger, 1983). One may apply the method of stability analysis for parabolic equations to the iteration solutions for elliptic, steady state equations. In order to introduce a mathematical theory for stability analysis the following form of general matrix equation is used:

$$u' = A u + \text{others}.$$

According to the method of lines which approximates partial differential equations by the system of ordinary differential equations, the stability of this matrix system depends on the eigen values of matrix A. If the eigen values of matrix A are negative numbers or are complex numbers with negative real parts, any deviation during iteration is damped out on subsequent steps. That is, the system corresponding to the matrix equation is stable. In order to check the locations of eigen values on the complex plane, the Gêrsgorin disk theorem can be used. The Gêsgorin disk theorem states that all eigenvalues of a square matrix lie within the Gêrsgorin disks. The center of each Gêrsgorin disk is at the value of each diagonal element of matrix A and the radius is the sum of absolute values of off-diagonal elements in every row.

Patankar (Patankar, 1980) proposes four rules for development of numerical schemes. The first rule is consistency at control volume faces. It states that for a face common to two adjacent control volumes, the flux across the face must be represented by the same value in the discretization equations for the two control volumes.

The second rule relates to the sign of coefficients in the finite difference equation. This rule states that all coefficients should have the same sign.

Patankar's fourth rule is that the value of the coefficient of the variable at the computational node should be equal to the sum of all the off-diagonal coefficients. It derives from the fact that the governing differential equations contain only the derivatives of the dependent variables. In this case, the finite difference equation should be satisfied if a constant is added to the dependent variable.

One shall accept only those schemes that guarantee positive coefficients under all circumstances. Patankar's rules are more restrictive than the Gêrsgorin disk theorem because Patankar's rule is only for real variables. Thus if Patankar's rules are satisfied, the Gêrsgorin disk always is located in the left half of complex plane.

The QUICK scheme (Leonard, 1979) was developed to get second order accuracy together with better numerical stability. The problems associated with central and upstream differencing schemes can be interpreted in terms of the method or estimating the values of the dependent variables on the faces of the control volume. For central differencing the estimation is based on linear interpolation. Upstream differencing is equivalent to zeroth order interpolation with the choice of direction depending on the sign for velocity. Quick uses quadratic polynomials to evaluate u_e on the faces of the control volume shown in Fig. 7. The quadratic polynomial, $u = a + bx + cx^2$, has three coefficients to be evaluated, which requires the values of u at three nodal points. Those three points are chosen in the upstream direction. If the direction of flow is from left to right, one needs the values of u_e at $I-1$, I and $I+1$.

For a uniform grid, the value of u_e becomes

$$\frac{1}{2}(u_I + u_{I+1}) - \frac{1}{8}(u_{I+1} + u_{I-1} - 2u_I)$$

which may be interpreted as a linear interpolation corrected by a term proportional to the upstream weighted curvature.

Applying the QUICK scheme to the one-dimensional model problem illustrates the instability of QUICK according to Patankar's second rule and fourth rule. The convective terms are:

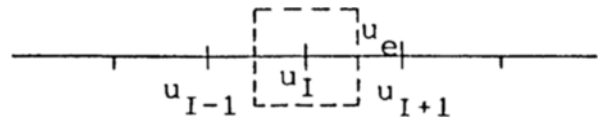

Fig. 7 Grid points and control volume

$$C_e u_e - C_w u_w = \left(\frac{3}{4}C_e - \frac{3}{8}C_w\right)u_I + \left(\frac{3}{8}C_e\right)u_{I+1} - \left(\frac{C_e}{8} + \frac{3}{4}C_w\right)u_I + \frac{1}{8}C_w\, u_{I-2}$$

where C_e is equal to C_w for one-dimensional flow. The convective terms can be reduced to

$$\frac{3}{8}Cu_I + \frac{3}{8}Cu_{I+1} - \frac{7}{8}Cu_{I-1} + \frac{1}{8}Cu_{I-2}$$

If the above equations are rearranged according to the general form of the finite difference equation, the result is

$$\frac{3}{8}Cu_I = -\frac{3}{8}Cu_{I+1} + \frac{7}{8}Cu_{I-1} - \frac{1}{8}Cu_{I-2}$$

The coefficients become

$$a_p = \frac{3}{8}C \quad a_e = -\frac{3}{8}C \quad a_w = \frac{7}{8}C \quad \text{others} = -\frac{1}{8}C$$

Combining the diffusion terms with the above formulation gives

$$a_p = \frac{3}{8}C + D_e + D_w \quad a_e = -\frac{3}{8}C + D_e \quad a_w = \frac{7}{8}C + D_w$$
$$\text{others} = -\frac{1}{8}C$$

where D is the diffusivity divided by a computational cell size. If the flow direction is positive, a_e may become negative, which violates Patankar's second rule. It leads Gêrsgorin disk to include the right hand side of plane. Thus QUICK is open to numerical instability for this formulation.

Han, et. al., (Han, 1981) evaluate the QUICK scheme by applying it to the simulation of laminar flow in a cavity. They redistribute the terms in the momentum equation to improve stability. Two formulations are shown below.

$$\begin{aligned} &u_e > 0 \quad u_e = \frac{1}{8}(-u_{I-1} + 6u_I + 3u_{I+1}) \\ &u_e < 0 \quad u_e = \frac{1}{8}(3u_I + 6u_{I+1}) - \boxed{\frac{1}{8}u_{I+2}} \end{aligned} \tag{2}$$

$$\begin{aligned} &u_e < 0 \quad u_e = \frac{1}{8}(3u_I + 4u_{I+1}) - \boxed{\frac{1}{8}(u_{I+2} - 2u_{I-1})} \\ &u_e > 0 \quad u_e = \frac{1}{8}(6u_I + 4u_{I+1}) - \boxed{\frac{1}{8}(u_{I-1} + u_{I+1})} \end{aligned} \tag{3}$$

where $\boxed{\ }$ denotes the terms treated as the source term in finite difference equations. The solution converges using Eq. (3). QUICK scheme was applied to simulated the recirculating turbulent flow through the sudden expansion. It was unstable in numerical calculations. Why this formulation is sometimes unstable is explained below by using Gêrsgorin Disk theorem.

An unrealistic, one-dimensional model problem without the diffusion terms is examined because it is capable of illustrating the worst case of instability. The convective terms are:

$u_e > 0$ and $u_w > 0$

$$C_e u_e - C_w u_w = C_e\left(\frac{6}{8}u_I + \frac{4}{8}u_{I+1}\right) - C_e\frac{1}{8}(u_{I-1} + u_{I+1}) - C_w\left(\frac{6}{8}u_{I-1} + \frac{4}{8}u_I\right) + C_w\frac{1}{8}(u_{I-2} + u_I)$$

where C_e is equal to C_w for one-dimensional flow. The convective terms can be reduced to

$$\frac{2}{8}Cu_I = -\frac{4}{8}Cu_{I+1} + \frac{6}{8}Cu_{I-1} + \frac{1}{8}C(u_{I-1} + u_{I+1}) - \frac{1}{8}C(u_{I-2} + u_I)$$

The coefficients become

$$a_p = \frac{2}{8}C, \quad a_e = -\frac{4}{8}C, \quad a_w = \frac{6}{8}C,$$

$$\text{others} = \frac{1}{8}C(u_{I-1} + u_{I+1}) - \frac{1}{8}C(u_{I-2} + u_I).$$

The center of the Gêrsgorin Disk is $-\frac{2}{8}C$ and the radius of disk is $|u_e| + |a_w|$ which is $\frac{10}{8}C$. This Gêrsgorin Disk is shown in Fig. 8.

It shows that the Disk includes the right side of the complex plane, so QUICK formulation with (3) is also open to numerical instability.

The new formulation of QUICK has been developed which has absoluted numerical stability (Absolutely Stable QUICK scheme). The upstream differencing scheme is absolutely stable although it yields only first order computational accuracy. The genesis of the idea is to maintain the numerical stability of upstream differencing and also to obtain a second order numerical accuracy through the source terms.

The value for u_e is approximated by the original QUICK in the upstream direction.

$$\begin{aligned} &u_e > 0 \quad u_e = \frac{1}{8}(-u_{I-1} + 6u_I + 3u_{I+1}) \\ &u_e < 0 \quad u_e = \frac{1}{8}(3u_I + 6u_{I+1} - u_{I+2}) \end{aligned}$$

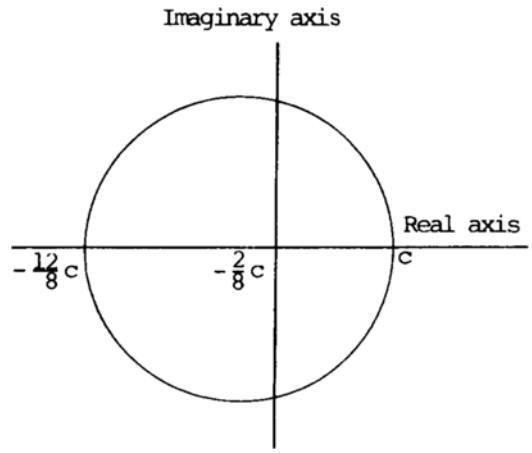

Fig. 8 Gêrsgorin disk

In the Absolutely Stable QUICK scheme, the above formulations are divided into two parts. One part represents UPSTREAM formulations, and the other part represents the correction terms necessary to obtain a second order accuracy. These formulations are:

$$u_e>0 \quad u_e=u_I+\boxed{\frac{1}{8}(-u_{I-1}-2u_I+3u_{I+1})}$$

$$u_e<0 \quad u_e=u_{I+1}+\boxed{\frac{1}{8}(3u_I-2u_{I+1}-u_{I+2})}$$

In iterative calculations, $\boxed{\ }$ denotes the terms treated as source terms in finite difference equations. This new form of QUICK has the desired numerical properties, consistency, positive coefficients of finite difference equations and second order accuracy. It also has absolute stability because the strong diagonal dominant matrix of coefficients in the system of finite difference equations leads to always locating the Gêrsgorin Disk on the left half of the plane.

The important advantages of this new formulation are to avoid inconvenient numerical experiments in order to find a good stable formulation and to get high convergence rates due to absolute stability.

The absolute stability may be illustrated by the Gêrsgorin Disk theorem. A one-dimensional model problem is chosen. The convective terms are:

$$u_e>0 \text{ and } u_w>0$$

$$C_eu_e-C_wu_w=C_eu_I+\frac{1}{8}C_e(-u_{I-1}-2u_I+3u_{I+1})$$
$$-C_wu_{I-1}-\frac{1}{8}C_w(-u_{I-2}-2u_{I-1}+3u_I)$$

where C_e is equal to C_w for one dimensional flow.

The terms become:

$$Cu_I=Cu_{I-1}-\boxed{\frac{1}{8}C(-u_{I-1}-2u_I+3u_{I+1})}$$
$$+\boxed{\frac{1}{8}C(-u_{I-2}-2u_{I-1}+3u_I)}$$

The coefficients are:

$$a_p=c \qquad a_e=0 \qquad a_w=c$$

Terms in $\boxed{\ }$ are treated as source terms in numerical calculation.

The center of Gêrsgorin Disk is $-C$ and the radius of it is C. The Gêrsgorin Disk for this case is located in the left half of plane in Fig. 9.

Therefore, one can conclude that all eigen values of finite difference equations are located on the negative side of the plane. All eigen values are negative, and the deviation of calculated values from the exact solution is always decaying as the iteration goes, which is absolute stability in numerical calculations.

The Absolutely Stable QUICK reduces numerical diffusion associated with upstream differencing by introducing correctional source terms. It is applied to modeling the fluid flow through a sudden expansion, which has a very strong recirculation zone. The formulation of linear, finite difference equations begins from the basis of the HYBRID difference scheme which has central and upstream differencing. Central differencing is used when the cell Reynolds number is less than 2. It has second order accuracy and does not have numerical diffusion problems. Upstream differencing is used when the cell Reynolds number is greater than 2. It has only first order accuracy with attendant numerical diffusion. Additional source terms are added to subtract numerical diffusion and to obtain second order accuracy. These additional source terms are the correction terms for numerical diffusion from upstream differencing. Absolutely Stable QUICK is stable in numerical calculations and shows a good convergence rate.

The reattachment length predicted by the Absolutely Stable QUICK is compared with that obtained using the HYBRID scheme. For flow through a sudden expansion with an expansion ratio of 2.24 and Reynolds number of 103,000, the reattachment length predicted by the HYBRID scheme is 3.69 meter while that predicted by the new scheme is 4.19 meter. A numerical experiment is done with a finer grid system using the HYBRID scheme in order to check the trends predicted by the Absolutely Stable QUICK. The HYBRID schme using a grid spacing reduced by 2 predicts a reattachment length of 3.92 meter. The extended length of the

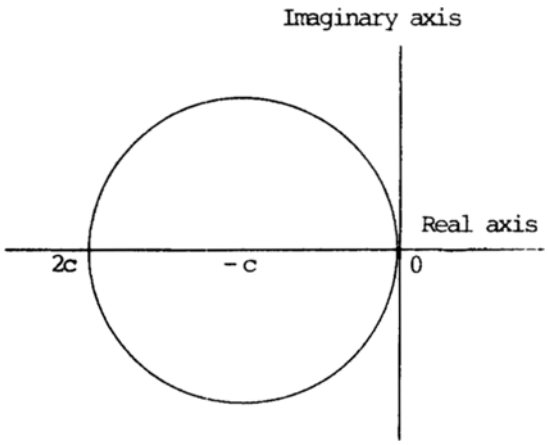

Fig. 9 Gêrsgorin disk

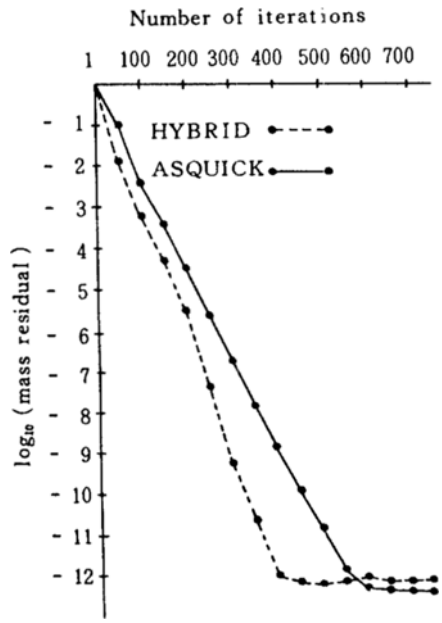

Fig. 10 Comparision of convergence rates

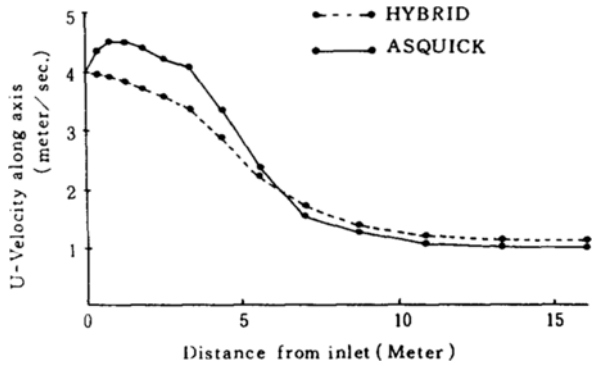

Fig. 11 Centerline velocity

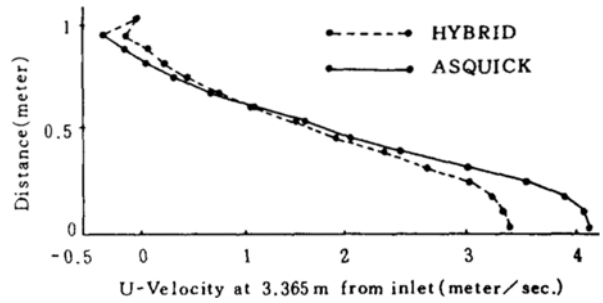

Fig. 12 Velocity profile in radial direction

recirculation zone is consistent with the reduction in numerical diffusion obtained by using the Absolutely Stable QUICK. This is consistent with McGuirk (McGuirk, 1981) who finds that the length of the recirculation zone is increaed with reduced numerical diffusion. The comparision of the convergence rate between HYBRID and Absolutely Stable QUICK is shown in Fig. 10. Absoluteiy Stable QUICK requires about 20% to 40% more iterations than HYBRID, which is 10% to 30% faster convergence than Humphrey's QUICK (Han, 1981). Absolutely Stable QUICK leads to less mass residual at the end of calculations than HYBRID. The centerline velocity distribution and the velocity profiles in the radial direction predicted by the Absolutely Stable QUICK are plotted in Fig. 11 and Fig. 12, respectively, and compared with the predictions using the HYBRID scheme. There are noticeable differences among predictions, which are consistent with the change of reattachment length. The magnitude of u-velocity along the axis predicted by Absolutely Stable QUICK is higher in the region of recirculation than that predicted by the HYBRID scheme.

2.4 Numerical Procedure

Finite difference formulations of the governing equations are developed from the conservative form of the equations. A volumetric integration of the governing equations is taken over a computational cell which is formed by the curvilinear grid lines. This grid system, called the standard grid system in this work, is used for the calculation of all dependent variables except for the u and v velocities. For the u and v velocities, a staggered grid system is formed by locating velocities midway on the link between two grid points instead of at grid points. The velocities are on the sides of each computational cell. The calculation of the w-velocity component, however, is done with the standard grid system because the flow field to be simulated has no pressure gredients in the direction of the w-velocity due to axisymmetry.

$$\frac{1}{\ell_\xi \ell_\eta \ell_\zeta}\frac{\partial}{\partial \zeta}(\ell_\eta \ell_\zeta \rho u \phi) + \frac{1}{\ell_\xi \ell_\eta \ell_\zeta}\frac{\partial}{\partial \eta}(\ell_\xi \ell_\zeta \rho v \phi)$$

$$= \frac{1}{\ell_\xi \ell_\eta \ell_\zeta}\frac{\partial}{\partial \xi}\left(\sqrt{\phi}\frac{\ell_\eta \ell_\zeta \partial \phi}{\ell_\xi \partial \xi}\right) + \frac{1}{\ell_\xi \ell_\eta \ell_\zeta}\frac{\partial}{\partial \eta}\left(\sqrt{\phi}\frac{\ell_\xi \ell_\zeta \partial \phi}{\ell_\eta \eta}\right) + s_\phi,$$

where ϕ, $\sqrt{\phi}$ and s_ϕ denoted the dependent variables, diffusion coefficients and source terms, respectively. The expressions of ϕ, $\sqrt{\phi}$ and s_ϕ are given in Table 1 and Table 2, where G represents turbulent energy generation. Energy dissipation terms are neglected in the source terms of thermal energy equation because the magnitude of dissipation term is much smaller than that of convective terms in subsonic flow (Schlichting, 1979). The Absolutely Stable QUICK scheme is used to formulate the system of the finited difference equations.

A line-by-line method is adopted to solve the system of finite difference equations iteratively. It is a convenient combination of the direct method and the Gauss-Seidel point-by-point method. The momentum equations are solved to get velocity fields and then a pressure-velocity correction equation from the continuity equation is solved to obtain pressure. Pressure fields and corrected velocity fields are obtained from the pressure-velocity correction equation. The turbulent energy and dissipation equations are solved next. These precedures are repeated until the mass residuals are less than a predetermined value.

The PISO (Pressure Implicit Split Operator) scheme as a pressure-velocity correction scheme is used in this work to reduce costly computational time. It was developed by Issa (Benodekar, 1983). It takes into accout the convective terms of the finite difference equation together with pressure terms for velocity corrections. Two stages of correction are used. The first stage of correction is accomplished by executing the SIMPLE scheme, and then the velocities are corrected again with the convective terms.

Neely and Claus (Neely, 1985) use the TEACH program and compare PISO with SIMPLE for turbulent flow over a backwardfacing step. They claim that PISO reduces computational time. The extent of recduction in computational time depends on the number of grid points. They states that the ratio between CPU time for SIMPLE and PISO decreases with the decreasing number of grid points.

Here, another comparison betwwen SIMPLE and PISO is

Table 1 Dependent variables and diffusion coefficients

Equation	ϕ	ϕ
Continuity	1	0
u-momentum	u	μ_t
v-momentum	v	μ_t
w-momentum	w	μ_t
Thermal energy	T	K
Turbulent energy	k	μ_t/σ_k
Turbulent dissipation	ε	μ_t/σ_ε
Concentration	s_x or w_x	D

Table 2 Source term in finite difference equation

Equation	S_ϕ
Continuity	0
Momentum	
u	$-\frac{\rho uv}{r_\xi}+\frac{\rho v^2}{r_\eta}+\frac{\rho w^2}{r_{\zeta\xi}}-\frac{\partial p}{\ell_\xi\partial\xi}+\frac{1}{\ell_\xi\ell_\eta\ell_\zeta}\frac{\partial}{\partial\xi}(\ell_\eta\ell_\zeta\mu(\frac{\partial u}{\ell_\xi\partial\xi}+\frac{2v}{r_\eta}))$ $+\frac{1}{\ell_\xi\ell_\eta\ell_\zeta}\frac{\partial}{\partial\eta}(\ell_\xi\ell_\zeta\mu(\frac{\partial v}{\ell_\eta\partial\xi}+\frac{v}{r_\xi}))+\frac{\tau_{\xi\eta}}{r_\xi}-\frac{\tau_{\eta\eta}}{r_\eta}-\frac{\tau_{\zeta\zeta}}{r_{\zeta\xi}}+\rho g_\xi$
v	$\frac{\rho u^2}{r_\xi}-\frac{\rho uv}{r_\eta}+\frac{\rho w^2}{r_{\zeta\eta}}-\frac{\partial p}{\ell_\eta\partial\eta}+\frac{1}{\ell_\xi\ell_\eta\ell_\zeta}\frac{\partial}{\partial\xi}(\ell_\eta\ell_\zeta\mu(\frac{\partial u}{\ell_\eta\partial\eta}-\frac{u}{r_\eta}-\frac{v}{r_\xi}))$ $+\frac{1}{\ell_\xi\ell_\eta\ell_\zeta}\frac{\partial}{\partial\eta}(\ell_\xi\ell_\zeta\mu(\frac{\partial v}{\ell_\eta\partial\eta}+\frac{2u}{r_\xi}))-\frac{\tau_{\xi\xi}}{r_\xi}-\frac{\tau_{\eta\xi}}{r_\eta}-\frac{\tau_{\zeta\xi}}{r_{\zeta\eta}}+\rho g_\eta$
w	$-\frac{\rho wv}{r_{\zeta\eta}}-\frac{\rho wu}{r_{\zeta\xi}}+\frac{1}{\ell_\xi\ell_\eta\ell_\zeta}\frac{\partial}{\partial\xi}(\ell_\eta\ell_\zeta\eta(-\frac{w}{r_{\zeta\xi}}))$ $+\frac{1}{\ell_\xi\ell_\eta\ell_\zeta}\frac{\partial}{\partial\eta}(\ell_\xi\ell_\zeta\mu(-\frac{w}{r_{\zeta\eta}}))+\frac{\tau_{\zeta\eta}}{r_{\zeta\eta}}+\frac{\tau_{\zeta\xi}}{r_{\zeta\xi}}$
Turbulent energy	$\mu_t G-C_D\rho\varepsilon$
Turbulent dissipation	$C_1\mu_t G\frac{\varepsilon}{k}-C_2\rho\frac{\varepsilon^2}{k}$
Thermal energy	0

done on the axisymmetric turbulent flow through a sudden expansion section of which the expansion ratio and Reynolds number are 2.24 and 103,000 respectively. The number of computational grid points is 240 (16×15 grid). The mass residuals are used as the convergence criteria. PISO shows a higher rate of convergence than SIMPLE. The reduction in the number of iterations using PISO instead of SIMPLE was about 8%, which is comparable to the results of Neely and Claus (Neely, 1985).

3. NUMERICAL SIMULATION OF DISPERSED PHASE

There are basically two approaches in the literature that have been used to model numerically the flow a dispersed phase: the Eulerian two-fluid approach and the Lagrangian trajectory approach.

In the Eulerian two-fluid model, the continuous phase and dispersed phase are treated as a continuum. The Eulerian form of momentum equations for the dispersed phase has neither pressure gradient term nor diffusion terms and has only coupling terms between two phases. There are several problems in the numerical simulations of the dispersed phase, one of which is numerical instability. In order to obtain stable numerical solutions, the upstream difference scheme has to be used for the momentum equations of dispersed phase even though it has only first order accuracy. Furthermore, it is noted by Crowe (Crowe, 1982) that numerical simulation of boundary conditions is troublesome and that the particle velocity in the computational cell may not be unique.

The trajectory approach utilizes the Eulerian equations for the continuous phase and the Lagrangian equations for the dispersed phase. There is no confusion concerning the velocity of dispersed phase in a computational cell even though two different droplets traverse the same computational volume because each trajectory of the dispersed phase is followed.

Durst (Durst, 1984) reports numerical experiment of and Lagrangian approaches for modeling particulate two-phase flow. He claims that the Lagrangian approache gives more detailed information on the particle phase, but it has convergence problem in case of high loading.

After considering the relative advantage and disadvantages, the Lagrangian trajectory approach was chosen for this study.

3.1 Absorption of Sulfur Dioxide

In spray dryer F. G. D., the spray of slurry droplets is formed by a atomizer. The slurries consist of line, chemical components from the flue gas and water. The size of droplets usually ranges from 10^{-4}m to 10^{-5}m. The atomized droplets both evaporate due to the high temperature of flue gas and absorb SO_2 as they pass through the chamber of the spray dryer. The atomized droplets first become wet porous particles and ultimately become dry.

The elementary processes involved in chemical absorption into a slurry droplet are: (i) diffusion of solute gas through the gas film, (ii) diffusion in the liquid film, (iii) chemical reaction, and (iv) dissolution of solids (one of the reactants). These transfer processes can occur either in parallel or series. If this transfer process is assumed to be serial, it can be analyzed in terms of conventional chemical absorption theories. If on the other hand, the process is assumed to be in parallel, the absorption rate is influenced and, infact, enhanced by the coexistence of solid dissolution, of which can be suspended in the liquid film. More specifically the rate of SO_2 dissolution is enhanced by the reaction between the gas and dissolved solid in the liquid film.

The reaction in flue gas desulfurization using a slurry droplet is regarded as being both serial and parallel. The evaluation of desulfurization rate, or the efficiency, is further complicated by the coexistence of the solid dissolution.

The only data available in the literature on the absorption of SO_2 by lime slurries are those reported by Sada (Sada,

1983). His experiments involve the absorption of dilute SO_2 into aqueous double slurries $CaCO_3$ and $Mg(OH)_2$ at 298 K and liquid interface. It is operated batchwise in the liquid phase and continuously in the gas phase.

The absorption rate increases with time the corresponding SO_2 concentration decreases, and the reaction finally reaches the condition in which the process is completely gasfilm controlled. Some fraction of the sulfur dioxide absorbed in the double slurry is accumulated as the $MgSO_3^0$ ion pair, and it is believed that this ion pair is responsible for the increased absorption rate.

Sada's results suggest that in spray dryer F. G. D. applications, where the slurry is recirculated, the dissolved sulfur dioxide reacts mainly with the $MgSO_3^0$ ion pair, and the absorption rate into slurry droplets is completely controlled by the gas-film mass transfer resistence.

The absorption of sulfur dioxide into wet porous particles is complicated by the gaseous diffusion in the pores, the reaction within the porous particles and the solid state diffusion. There is no data available for this particular case. In this report, the absorption of sulfur dioxide into the wet porous particles is neglected because the absorption phenomena is assumed as a process controlled by solid state diffusion, which is much slower than gas state diffusion. A reliable model for sulfur dioxide absorption into wet porous particles, however, is needed.

Bhatia's (Bhatia, 1981) studies involve the SO_2 absorption into bone dry particles. He concludes that the absorption rate is controlled by solid state diffusion, and the absorption rate of SO_2 by dry particles is much smaller than that by the gas phase mass transfer controlled process. Absorption into dry particles is neglected in this report.

Mass transfer through the gaseous phase is modeled by the equation.

$$\dot{m} = sh(\rho D)\pi d_p(X_v - X_\infty)$$

where ρ is the density of the fule gas, D is the binary diffusivity in the flue gas, X_v is the mass fraction at the surface of droplet, X_∞ is the mass fraction in the flue gas, and d_p is the droplet diameter. The mass fraction of SO_2 at the droplet surface is evaluated according to Crawford's book (Crawford, 1976) and Sada's data. The details are available in Kim's work (Kim, 1985). One obtains a relative sulfur dioxide mass fraction of 0.001 at the surface of the droplets with respect to X_∞. For this work, X_v is assumed zero.

3.2 Development of Governing Equation

The governing equations are developed according to the method described in Crowe's study (Crowe, 1983). They consist of a momentum equation, a mass balance equation and a heat balance equation. The equations are descibed in detail in Kim (Kim, 1985). In this work, the steady state aerodynamic drag is the dominant force acting on the droplet. All other forces (Basset force, Magnus force and Saffman life force) are neglected because the ratio of the density of the continuous phase to that of the dispersed phase is small. Also, the velocity gradients are not large enough to cause a significant Saffman lift force. Semi-implicit numerical integration of the equations are taken to obtain the droplet velocities. The centrifugal and Coriolis acceleration terms are treated as source terms in the numerical integration (See Kim (Kim, 1985)).

The size of the droplet is calculated by considering mass balance in a droplet. The evaporation of water can be modeled by consecutive two-stage processes. The two stages consist of the constant rate period and the falling rate period. For the constant rate period, the rate of decrease of particle mass is given by:

$$m_s dw/dt = -\dot{m}_1 - \dot{m}_2$$
$$\dot{m}_1 = sh_1(\rho D_1)\pi d_p(x_{1v} - x_{1\infty}),$$
$$\dot{m}_2 = sh_2(\rho D_2)\pi d_p(x_{2v} - x_{2\infty})$$

where w is the ratio of m_l/m_s, m_l and m_s are the mass of the liquid and the mass of the solid particles in the droplet, x_v is the mass fraction at the surface, and x_∞ is the mass fraction in the free stream: the subscripts 1 and 2 denote water and sulfur dioxide, respectively.

For the falling rate period, dw/dt is assumed to be proportional to the liquid content in the droplets:

$$dw/dt = k(w - w_e)$$

where k is the proportinality constant and is equal to the evaporation rate calculated at the critical liquid content, which is set to 0.3. w_e is the equilibrium liquid content, which is assumed to be zero. The equations used for droplet diameter and temperature are available through another source (Kim, 1985).

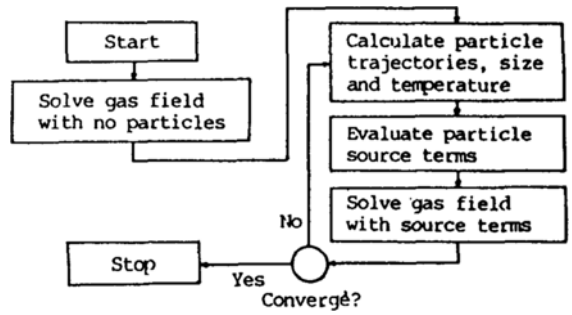

Fig. 13 Flow chart

3.3 PSI-CELL Scheme

The PSI-CELL scheme developed by Crowe and his associates (Crowe, 1977) in 1977 is a Lagrangian trajectory approach. It is founded on the idea of treating the dispersed phase as sources of mass, momentum and energy to the continuous phase. These source terms come from the coupling of two phases, so called, two-way coupling.

The numerical solutions for the dispersed and continuous phases are obtained according to the flow diagram shown in Fig. 13.

4. THE SPRAY DRYER F.G.D. PROGRAM

The program is developed and is applied to the prediction of sulfur dioxide absorption and the gas-droplet flow phenomena in typical F. G. D. spray dryer configulation. The spray dryer is 18.11 m high. The diameter at the top is 5.4m and the outlet diameter is 1.27m. The conical contraction section startes at 7.32m from the top. The inlet diameter for flue gas is 1.79m. The nominal run conditions, shown in Table 3, are used for the numerical experiments.

The predicted velocity field in the traverse plane is shown

Table 3 Normal run conditions

Atomizer wheel diameter (cm)	29.3
Atomized wheel speed (rpm)	10891.
Gas inlet vertical velocity (m/sec)	17.3
Gas inlet swirl velocity (m/sec)	4.3
Gas inlet relative humidity (%)	1.
Gas inlet SO_2 concentration (ppm)	1500
Gas inlet temperature (K)	403
Loading of droplets in flue gas	0.0146
Inlet slurry temperature (K)	324.
Mass ratio between solid lime and water	0.15.
Droplets size distribution (micron)	40, 60, 80
Mass distribution for each size range (%)	25, 50, 25
Initial droplet injection velocity (m/sec)	167.

in Fig. 14, illustrating the recirculation zone produced by the sudden expansion section.

The radial distribution of the u-velocity at two diameter downstream from the inlet is shown is Fig. 15. One notes the reversal of velocity corresponding to the recirculation zone. The predictions with and without droplets in the flow show little effect of the droplets in the u-velocity field. The velocity fields of v and w also show similar trends.

Typical droplet trajectories in the spray dryer are shown in Fig. 16. The droplets emerge radially from the atomizer wheel and are quickly deflected in the axial direction by the gas stream. One also notes that the larger droplets penetrate farther into the flow.

The change of sulfur dioxide concentration in the flue gas along the trajectory of a droplet is shown in Fig. 17. The absorption rate is higher near the injection point. This trend arises because the concentration is initially high, and the mass transfer is enhanced by the relative velocity between the droplets and gas. Finally the droplet drys to a wet porous particles and the absorption ceases. The curves, then, rise because sulfur dioxide diffuses to the low concentration region around the trajectories.

The water content in the droplet as a function of distance along the trajectory for 40 micron droplets is shown in Fig. 18. The water content decreases very quickly at the beginning. At the highest temperature, 1003 k, the droplets dry to

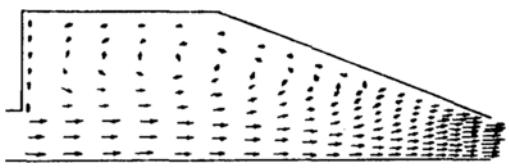

Fig. 14 Velocity field

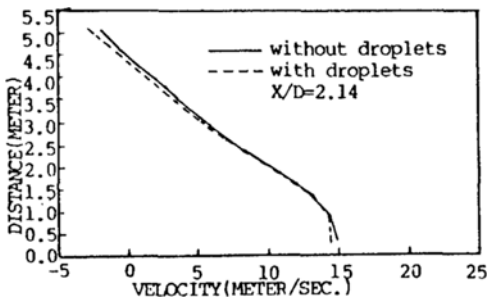

Fig. 15 u-velocity

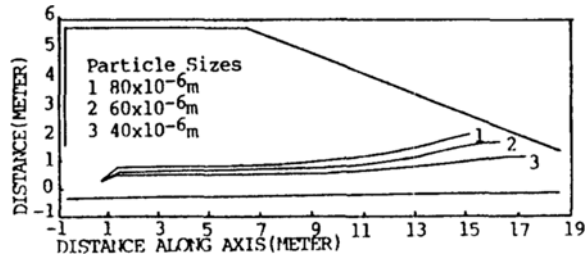

Fig. 16 Droplet trajectories

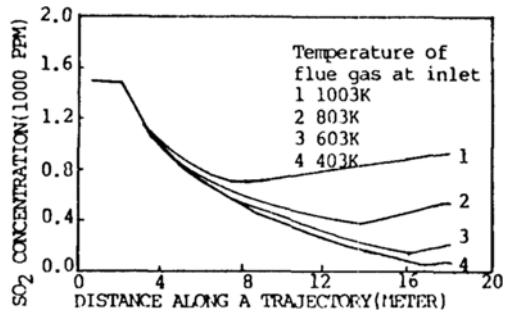

Fig. 17 Change of sulfur dioxide in the gas along the trajectory.

the wet porous particles approximately halfway through the spray dryer. The absorption model is no longer accurate after this point.

The concentrations of sulfur dioxide at the outlet as a function of inlet gas temperature is shown in Fig. 19. One notes that the concentration increases with increasing temperrature because the droplets dry more quickly and are less effective in absorbing sulfur dioxide.

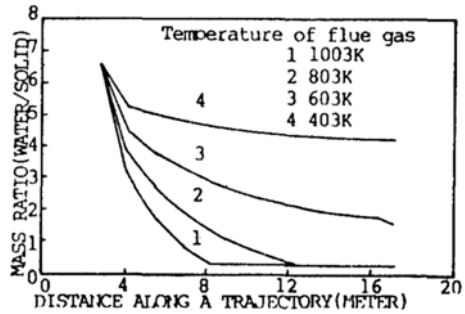

Fig. 18 The change of water content in a droplet

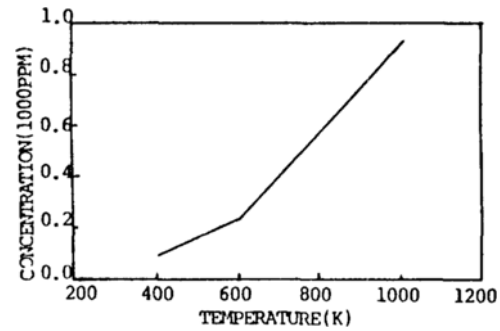

Fig. 19 The variation of sulfur dioxide concentration at the outlet with the inlet temperature of flue gas

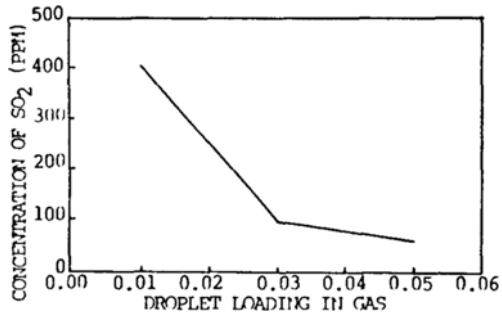

Fig. 20 The variation of sulfur dioxide concentration at the outlet with loading of droplets in the flue gas

The variation of the sulfur concentration at the outlet with the droplet loading in the flue gas is shown in Fig. 20. The concentration is decreased with increased loading because of the larger droplet surface area.

5. CONCLUSION

The developed computational program based on the Lagrangian trajectory approach to the dispersed phase is capable of predicting the sensitivity of system performance to changes in operational parameters. The Absolutly Stable QUICK scheme is proven to be absolutly stable in numerical calculations by a mathematical theory, and it exhibit a good convergence rate. A mass transfer controlled model simulates reasonably well the chemical absorption process of sulfur dioxide to slurry droplets.

For future research directions on the numerical modeling of the spray dryer flue gas desulfurization system, the following points are recommended:

(1) Develop a suitable turbulence model for anisotropic turbulent flow.
(2) Develop an economical, reliable method for simulating numerically particle dispersion in turbulent flow.
(3) Develop a model of sulfur dioxide absorption into wet porous particles.

ACKNOWLEDGMENT

The author is grateful to the Korean Science & Engineering Foundation and the Korea Research Foundation for supporting this work.

REFERENCE

Benodekar, R. W., Goddard, A. J. H., Gosman, A. D., 1983, "Numerical Prediction of Turbulent Flow over Survace Mounted Ribs", 83-FE-13, ASME.

Bhatia, S. K. and Perlmutler, D. D., 1981 "The Effect of Pore Structure on Fluid-Solid Reactions Application to SO_2-Lime Reaction", AICHE J. 27, pp. 226~234.

Christian, S., 1982, "The Science and Art of Spray Dryer Design for Flue Gas Desulfurization", Coal Technology '82' Astrohall, Houston, Texas, Dec 7-9.

Crawford, M., 1976, "Art Pollution Control Theory", McGraw-Hill, Inc., pp. 463~506.

Crowe, C. T., 1982, "Review-Numerical Models for Dilute Gas-Particle Flows", J. of Fluid Engineering, Vol. 104, pp. 297~303.

Crowe, C. T. et al, 1977, "The Particle Source In Cell (PSI-CELL) Model for Gas Droplet Flows", Jnl Fluide Engr, Vol. 99, No. 2, pp. 325~332.

Crowe, C. T., 1983, 1984, "Droplet-Gas Interaction in Counter-Current Spray Dryer", Drying Technology, Vol. 1, No. 1, pp. 35~36.

Dukowicz, J. K., 1980 "A Particle-Fluid Numerical Model for Liquid Sprays", J. of Computational Physics, Vol. 35, pp. 229~253.

Durst, F. et al, 1984, "Eulerian and Lagrangian Predictions of Particulate Two-Phase Flows: A Numerical Study", Appl. Math. Modelling, Vol. 8, pp. 101~115.

Han T. et al, 1981, "A Comparison of Hybrid and Quadratic-Upstream Differencing in High Reynolds Number Elliptic Flows", Computer Methods in Applied Mechanics and Engineering, Vol. 29, pp. 81~95.

Kim, S. J., 1985, "A Numberical Model for Flue Gas Desulfurization System", Ph. D. Thesis, WSU.

Leonard, B. P., 1979, "A Stable and Accurate Convective Modelling Procedure Based on Quadratic Upstream Interpolation", Computer Methods in Applied Mechanics and Engineering, Vol. 19 pp. 59~98.

McGuirk, J. J. et al, 1981, "The Assessment of Numerical Diffusion in Upstream Difference Calculation of Turbulednt Recirculating Flows", Turbulent Shear Flows, Vol. 3, pp. 206~223.

Murthy, J., 1981, "Program for Generation of Orthogonal Curvilinear Grid System", Report No. 81-17, M. E., WSU.

Neely, G. M. and Claus, R. W., 1985, "Accelerated Convergence for Incompressible Flow Calculation", NASA TM-86873.

Neuberger, A. W. et al, 1983, "Selection of Relaxation Factors for Computing Steady State Turbulent Flows", Numerical Methods in Laminar and Turbulent Flow (Preceedings of The Third International Conference held at Seattle), pp. 280~289.

O'Rourke, R. T. and Wadt, W. R., 1982, "A Two Dimension Two-phase Numerical Model for Spray Dryer", LA-9423-MS, Los Alamos National Laboratory.

Patankar, S. V., 1980, "Numerical Heat Transfer and Fluid Flow", McGraw-Hill Book Co., pp. 36~39.

Pope, S. B., 1978, "The Calculation of Turbulent Recirculating Flows in General Orthogonal Coordinate", J. of Computational Physics, Vol. 26, pp. 197~217.

Sada, E. et al, 1983, "Absorption of Sulfur Dioxide into Aqueous Double Slurries Containing Limestone and Magnesium Hydroxide", AICHE J., Vol. 29, pp. 60~65.

Schlichting, H., 1979, "Boundary-Layer Theory", Seventh Edition, McGraw-Hill Book Co.

APPENDIX A

Constitutive equations

$$\tau_{\xi\xi}=2\mu\left(\frac{\partial u}{\ell_\xi\partial\xi}+\frac{v}{r_\eta}\right) \qquad \tau_{\xi\eta}=\mu\left(\frac{\partial u}{\ell_\eta\partial\eta}-\frac{u}{r_\eta}+\frac{\partial v}{\ell_\xi\partial\xi}-\frac{v}{r_\xi}\right)$$

$$\tau_{\eta\eta}=2\mu\left(\frac{\partial v}{\ell_\eta\partial\eta}+\frac{u}{r_\xi}\right) \qquad \tau_{\xi\zeta}=\mu\left(\frac{\partial w}{\ell_\xi\partial\xi}-\frac{w}{r_{\zeta\xi}}\right)$$

$$\tau_{\zeta\zeta}=2\mu\left(\frac{u}{r_{\zeta\xi}}+\frac{v}{r_{\zeta\eta}}\right) \qquad \tau_{\eta\zeta}=\mu\left(\frac{\partial w}{\ell_\eta\partial\eta}-\frac{w}{r_{\zeta\eta}}\right)$$

Continuity equation

$$\frac{1}{\ell_\xi \ell_\eta \ell_\zeta}\frac{\partial}{\partial \xi}(\rho u \ell_\eta \ell_\zeta)+\frac{1}{\ell_\xi \ell_\eta \ell_\zeta}\frac{\partial}{\partial \eta}(\rho v \ell_\xi \ell_\zeta)=0$$

General scalar transport equation

$$\frac{1}{\ell_\xi \ell_\eta \ell_\zeta}\frac{\partial}{\partial \xi}(\rho u \phi \ell_\eta \ell_\zeta)+\frac{1}{\ell_\xi \ell_\eta \ell_\zeta}\frac{\partial}{\partial \eta}(\rho v \phi \ell_\xi \ell_\zeta)$$
$$=-\frac{1}{\ell_\xi \ell_\eta \ell_\zeta}\frac{\partial}{\partial \xi}(q_\xi \ell_\eta \ell_\zeta)-\frac{1}{\ell_\xi \ell_\eta \ell_\zeta}\frac{\partial}{\partial \eta}(q_\eta \ell_\xi \ell_\zeta)+s$$

U-momentum equation

$$\frac{1}{\ell_\xi \ell_\eta \ell_\zeta}\frac{\partial}{\partial \xi}(\ell_\eta \ell_\zeta \rho u^2)+\frac{1}{\ell_\xi \ell_\eta \ell_\zeta}\frac{\partial}{\partial \eta}(\ell_\xi \ell_\zeta \rho u v)+\frac{\rho u v}{r_\xi}-\frac{\rho v^2}{r_\eta}$$
$$-\frac{\rho w^2}{r_{\zeta\xi}}$$
$$=-\frac{\partial p}{\ell_\xi \partial \xi}+\frac{1}{\ell_\xi \ell_\eta \ell_\zeta}\frac{\partial}{\partial \xi}(\ell_\eta \ell_\zeta \tau_{\xi\xi})+\frac{1}{\ell_\xi \ell_\eta \ell_\zeta}\frac{\partial}{\partial \eta}(\ell_\xi \ell_\zeta \tau_{\eta\xi})$$
$$+\frac{\tau_{\xi\eta}}{r_\xi}-\frac{\tau_{\eta\eta}}{r_\eta}-\frac{\tau_{\zeta\zeta}}{r_{\zeta\xi}}+\rho g_\xi$$

V-momentum equation

$$\frac{1}{\ell_\xi \ell_\eta \ell_\zeta}\frac{\partial}{\partial \xi}(\ell_\eta \ell_\xi \rho u v)+\frac{1}{\ell_\xi \ell_\eta \ell_\zeta}\frac{\partial}{\partial \xi}(\ell_\xi \ell_\zeta \rho v^2)-\frac{\rho u^2}{r_\xi}+\frac{\rho u v}{r_\eta}$$
$$-\frac{\rho w^2}{r_{\zeta\eta}}$$
$$=-\frac{\partial p}{\ell_\eta \partial \eta}+\frac{1}{\ell_\xi \ell_\eta \ell_\zeta}\frac{\partial}{\partial \xi}(\ell_\eta \ell_\xi \tau_{\xi\eta})+\frac{1}{\ell_\xi \ell_\eta \ell_\zeta}\frac{\partial}{\partial \xi}(\ell_\xi \ell_\zeta \tau_{\eta\eta})$$
$$-\frac{\tau_{\xi\xi}}{r_\xi}-\frac{\tau_{\eta\xi}}{r_\eta}-\frac{\tau_{\zeta\xi}}{\tau_{\zeta\eta}}+\rho g_\eta$$

W-momentum equation

$$\frac{1}{\ell_\xi \ell_\eta \ell_\zeta}\frac{\partial}{\partial \xi}(\ell_\eta \ell_\zeta \eta u w)+\frac{1}{\ell_\xi \ell_\eta \ell_\zeta}\frac{\partial}{\partial \xi}(\ell_\xi \ell_\zeta \rho v w)+\frac{\rho w v}{r_{\zeta\eta}}+\frac{\rho w u}{r_{\zeta\xi}}$$
$$=\frac{1}{\ell_\xi \ell_\eta \ell_\zeta}\frac{\partial}{\partial \xi}(\ell_\eta \ell_\xi \tau_{\xi\zeta})+\frac{1}{\ell_\xi \ell_\eta \ell_\zeta}\frac{\partial}{\partial \xi}(\ell_\xi \ell_\zeta \tau_{\eta\zeta})+\frac{\tau_{\zeta\eta}}{r_{\zeta\eta}}+\frac{\tau_{\zeta\xi}}{r_{\zeta\xi}}$$

Thermal energy equation

$$\frac{1}{\ell_\xi \ell_\eta \ell_\zeta}\frac{\partial}{\partial \xi}(\ell_\eta \ell_\zeta \rho u i)+\frac{1}{\ell_\xi \ell_\eta \ell_\zeta}\frac{\partial}{\partial \eta}(\ell_\xi \ell_\zeta \rho v i)$$
$$=-\frac{1}{\ell_\xi \ell_\eta \ell_\zeta}\frac{\partial}{\partial \xi}(\ell_\eta \ell_\zeta \rho_\xi)-\frac{1}{\ell_\xi \ell_\eta \ell_\zeta}\frac{\partial}{\partial \eta}(\ell_\xi \ell_\zeta q_\eta)$$
$$-P\left(\frac{1}{\ell_\xi \ell_\eta \ell_\zeta}\frac{\partial}{\partial \xi}(\ell_\eta \ell_\zeta u)+\frac{1}{\ell_\xi \ell_\eta \ell_\zeta}\frac{\partial}{\partial \eta}(\ell_\xi \ell_\zeta v)\right)$$
$$+\tau_{\xi\xi}\frac{\partial u}{\ell_\xi \partial \xi}+\tau_{\xi\eta}\frac{\partial u}{\ell_\eta \partial \eta}+\tau_{\xi\eta}\frac{\partial v}{\ell_\xi \partial \xi}+\tau\eta\eta\frac{\partial v}{\ell_\eta \partial \eta}$$
$$+\tau_{\xi\zeta}\frac{\partial w}{\ell_\xi \partial \xi}+\tau_{\eta\eta}\frac{\partial w}{\ell_\eta \partial n}+u\left(-\frac{\tau_{\xi\eta}}{r_\xi}+\frac{\tau_{\eta\eta}}{r_\eta}+\frac{\tau_{\zeta\xi}}{r_{\zeta\xi}}\right)$$
$$+v\left(\frac{\tau_{\xi\xi}}{r_\xi}+\frac{\tau_{\eta\xi}}{r_\eta}+\frac{\tau_{\zeta\xi}}{r_{\zeta\eta}}\right)-w\left(\frac{\tau_{\zeta\eta}}{r_{\zeta\eta}}+\frac{\tau_{\zeta\xi}}{r_{\zeta\xi}}\right)$$